Nanoscale

PAPER

View Article Online
View Journal | View Issue

Cite this: *Nanoscale*, 2017, **9**, 16200

Contrasting water adhesion strengths of hydrophobic surfaces engraved with hierarchical grooves: lotus leaf and rose petal effects†

Zhengqing Zhang,[a] Man Yeong Ha[b] and Joonkyung Jang *[a]

Received 3rd August 2017,
Accepted 22nd September 2017

DOI: 10.1039/c7nr05713j

rsc.li/nanoscale

The (de)wetting transitions of hierarchical grooves periodically engraved on a hydrophobic surface were investigated using a fully atomistic molecular dynamics simulation. The (meta) stable and transition states with sagging or depinning liquid surfaces were identified by calculating the free energy profiles of the (de)wetting transitions. The dewetting transitions for wide and narrow minor grooves have large and small activation free energies, respectively, exhibiting contrasting water adhesion forces as found for rose petals and lotus leaves.

Introduction

A hydrophobic surface engraved with hierarchical grooves is used in many applications, including antifouling,[1,2] antifogging,[3] and water/oil separation.[4–7] Such a grooved surface mimics the superhydrophobic surface of a lotus leaf or a rose petal,[8–12] which exhibits a high contact angle (>150°) with a water drop.[13] A water drop easily rolls off a lotus leaf[14] but adheres strongly to a rose petal.[15] These super-hydrophobic effects with contrasting adhesive forces of water are termed the lotus leaf and rose petal effects. The lotus effect is utilized for the self-cleaning properties of a surface, and a surface exhibiting the rose petal effect is used for liquid transportation,[16,17] wettability control,[18] and biochemical separation.[19]

Both the contact angle and adhesion strength of a water drop on a grooved surface depend critically on whether the underlying grooves are filled with water or not: the so-called Wenzel (WZ)[20] and Cassie–Baxter (CB)[21] states of the drop, respectively, refer to the cases where the grooves are full and void of water. For a hierarchical groove, each of the major and minor grooves can be in the WZ or CB state, giving rise to four possible composite states. The lotus effect is associated with the composite state, where both the major and minor grooves are in the CB states (CB–CB state). The WZ–CB state, where the major and minor grooves are in the WZ and CB states, respectively, exhibits the rose petal effect.[15]

Although the WZ (CB) states are induced by the wetting (dewetting) transitions of the grooves, the current understanding of the (de)wetting transition is far from complete, particularly for a hierarchical groove. In addition to a thermodynamically stable state, metastable and transition states can exist in (de)wetting. In particular, the activation free energy of dewetting (WZ to CB) pertains to the water adhesion strength of a surface. Herein, this study examined these aspects of the (de) wetting transitions by constructing the free energy profiles for rectangular hierarchical grooves (Fig. 1), which are common in experiments.[9] A fully atomistic molecular dynamics (MD) simulation was used, which, unlike the continuum theories,[22,23] obviates having to speculate the surface profile of a liquid in the wetting. The present simulation also provides discrete molecular features, such as the layering of water molecules near the solid surfaces.[24] A sagging or depinning surface of the liquid in

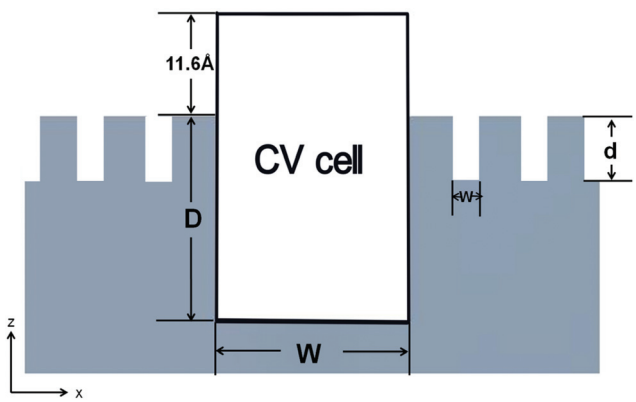

Fig. 1 Geometric parameters of a hierarchical groove. Shown is the cross section of an infinitely long and rectangular groove replicated periodically along the *X* axis. The depth and width of the major groove are represented as *D* and *W*, respectively. Multiple minor grooves with a height (*d*) and width (*w*) are also engraved. The collective variable (CV) cell used for the free energy calculation in the restrained MD simulation extends to a height of 11.6 Å above the top of the groove.

[a]*Department of Nanoenergy Engineering, Pusan National University, Busan 46241, Republic of Korea. E-mail: jkjang@pusan.ac.kr*
[b]*School of Mechanical Engineering, Pusan National University, Busan 46241, Republic of Korea*

†Electronic supplementary information (ESI) available. See DOI: 10.1039/c7nr05713j

wetting was uncovered. Substantially lower and higher activation free energies of dewetting were found with thin and wide minor grooves, respectively. These are related to the lotus leaf and rose petal effects.

Simulation methods

An infinitely long and rectangular groove with a width, W, was carved out of the face-centered cubic lattice of carbon atoms[24] and replicated by applying the periodic boundary conditions (PBCs) (Fig. 1). A hierarchical groove was constructed by engraving multiple minor grooves of a depth (d) and width (w), respectively. With W fixed to 23.2 Å, w^*s of 0.233 and 0.384 and d^*s of 0.2, 0.4, 0.8, 0.83, and 0.88 were simulated. Three, five, or nine minor grooves were engraved per single major groove to emulate both sparse and dense minor grooves.

Water molecules were modeled using the extended simple point charge model (SPC/E).[25] The long-range Coulomb interactions between point charges were handled using the particle–particle particle–mesh method.[26] The interactions between carbon and water oxygen atoms were modeled using the Lennard-Jones (LJ) potential with the size and well-depth parameters of 3.190 Å and 0.4389 kJ mol^{-1}, respectively.[24] Both the LJ and Coulomb interactions were truncated at a distance of 12 Å. Each grooved surface was covered with a layer of water with a thickness of 58.8 Å (4030 water molecules). A vacuum slab, 20–30 Å in thickness, was added on top of the water layer to remove the interactions between the water layer and the periodic images of the surface.[27] The MD trajectories were propagated using the velocity Verlet algorithm[28] with a time step of 2.0 fs. The rigid water molecules were simulated using the SHAKE algorithm[29] and all the carbon atoms were frozen. A 3.0 ns long MD simulation was run at 300 K using the Nosé–Hoover thermostat,[30,31] and the final configuration was used as the initial condition for the subsequent free energy calculation.

The potential of mean force (PMF) was calculated by controlling the number of water molecules inside a collective variable (CV) cell (Fig. 1). Using the umbrella sampling,[32] the number of water molecules inside the CV cell N was restrained to a target value by imposing a harmonic potential with a force constant of 0.05 or 0.12 kcal mol^{-1}. Typically, 75 windows were used to achieve sufficient overlap between the neighboring histograms. In each window, MD simulations were run for 10 ns and the initial 2 ns for equilibration were discarded. The PMF was extracted using the weighted histogram analysis method.[33–35] N was converted to the filling level Z using

$$Z = \frac{N - N_{CB}}{N_{WZ} - N_{CB}} \quad (1)$$

where N_{CB} and N_{WZ} are the number of water molecules inside the CV cell in the CB and WZ states, respectively. By construction, the CB and WZ states have Z = 0 and 1, respectively. All the MD simulations were performed using the LAMMPS[36] combined with the PLUMED[37] package.

Results and discussion

This study examined how water penetrates down into single-scale grooves. A liquid penetrates through either sagging (Fig. 2, top)[38,39] or depinning (Fig. 2, bottom)[40–42] by increasing the filling level Z (see Simulation methods for definition) from 0 to 1. For a groove with a relatively small depth D of 7.1 Å, the initially flat surface of the liquid develops a downward parabolic curvature while being pinned at the top edges of the groove (by changing Z from 0.02 to 0.30). With a further increase in Z, the liquid surface becomes sharper in curvature. The liquid surface eventually touches the groove bottom at Z = 0.75, and fully wets the groove (at Z = 1.00, WZ state). For a deeper groove with D = 23.2 Å, the liquid surface is depinned from the top edges of the groove (by increasing Z from 0.20 to 0.39). With further increases in Z, the liquid surface slides down the side walls without changing its curvature. This way, the liquid surface finally touches the bottom. Experimental observations of the sagging[38,39] and de-pinning[40–42] of liquids have also been reported.

Fig. 2 shows that the bottom corners of the grooves are not fully wet in the WZ states, particularly for a deeper groove. Further wetting increases the free energy of the grooves (see below). The same behavior is found for other grooves with D values of 8.9, 10.7, and 14.3 Å (see Fig. S1 in the ESI†). Note that the density near 2.8 Å away from the groove surface is partially depleted. This arises from the layering of water molecules near the groove surface. A depleted water density at a similar distance was observed in previous MD simulations.[24] The depinning or sagging of the penetrating liquid depends on which of the WZ and CB states is more stable: sagging (depinning) of the liquid surface is observed if the WZ (CB) state is stable. The same depinning and sagging behaviors for the hierarchical grooves were observed.

Fig. 3 presents the free energy profile of wetting, the PMF *vs.* Z, for hierarchical grooves with different depths. The width w^* and depth d^* of a minor groove are defined relative to the corresponding values of the major groove, W and D, respectively (therefore, w^*, $d^* < 1$). The minor grooves of these grooves

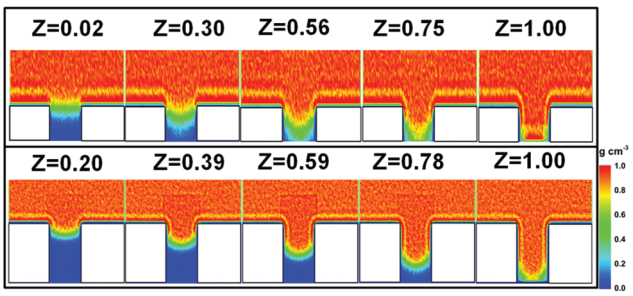

Fig. 2 Sagging and depinning surfaces of liquids in the wetting transitions of nonhierarchical grooves. Shown in the top and bottom are grooves with depths of 7.1 and 23.2 Å, respectively. The density profiles of water molecules are drawn as color maps by varying the filling level Z. The same color map is used in all subsequent figures.

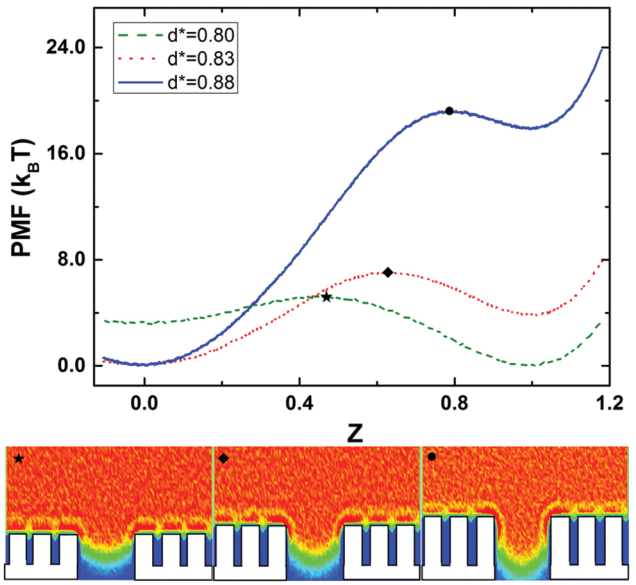

Fig. 3 Free energy profiles for the wetting transitions of the hierarchical grooves. The PMF is plotted *vs.* the filling level Z for minor grooves with depths, d^*s, of 0.80, 083, and 0.88. Five minor grooves with relative width, w^*, of 0.233 are engraved per single major groove. The density profiles of water at the transition states, which are marked as symbols in the PMF curves, are shown as color maps in the bottom.

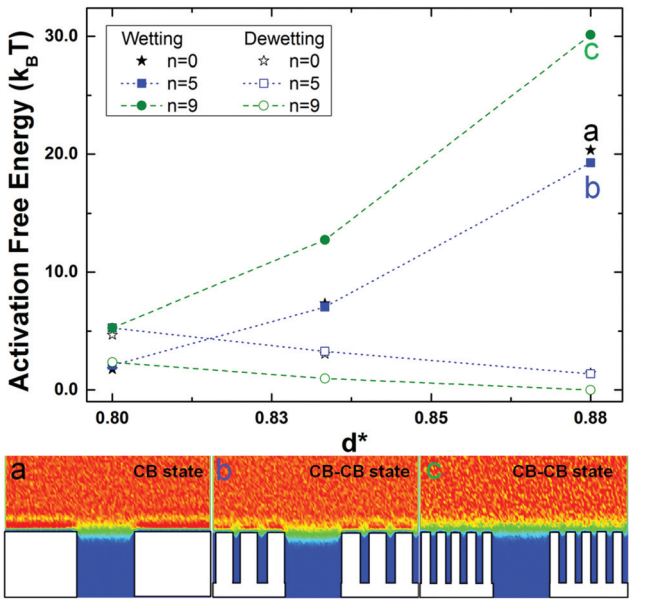

Fig. 4 Activation free energies of the wetting (filled symbols) and dewetting (empty symbols) transitions of the hierarchical grooves. The activation free energies of the grooves with different numbers of minor grooves are drawn *vs.* the minor groove depth (d^*). n represents the number of minor grooves per major groove. The lines serve as a visual guide only.

are always in the CB states. With increasing Z from 0 (CB–CB state), the PMF increases and culminates at the transition state marked by the symbol. With further increases in Z, the PMF decreased to another (local or global) minimum at Z = 1.0 (WZ–CB state). For grooves with d^* = 0.80, the WZ–CB (CB–CB) state is stable (metastable). With increasing d^* to 0.83 and 0.88, the CB–CB (WZ–CB) state becomes stable (metastable). The density profiles of the transition states are drawn in the bottom of Fig. 3. Here too, the liquid surfaces are sagged and depinned for relatively shallow (d^* = 0.80) and deep (d^* = 0.83 and 0.88) grooves, respectively. In addition, water molecules are layered near the top and sides of the major grooves, as manifested in the depletion of the density near the groove surfaces. The free energy profiles of the single-scale grooves (see Fig. S2 in the ESI†) are similar to those in Fig. 3.

The activation free energies (free energy barriers) of the wetting (CB-to-WZ) and dewetting (WZ-to-CB) transitions, which are drawn as filled and empty squares in Fig. 4, were calculated using the PMF curves shown in Fig. 3. The single-scale grooves and the hierarchical grooves with denser minor grooves were also simulated (see Table 1 for details). With increasing d^*, the activation free energies of the wetting and dewetting transitions increase and decrease, respectively. The activation free energies for the hierarchical grooves with relatively sparse (n = 5) minor grooves are virtually identical to those of the nonhierarchical grooves. With increasing density of the minor grooves (from n = 5 to n = 9), however, the activation free energies of the wetting and dewetting transitions increase (by 3–11k_BT) and decrease (by 1–3k_BT) significantly, respectively. The hierarchical grooves with the dense minor

Table 1 Geometrical parameters of the hierarchical grooves shown in Fig. 3 and 4. The relative depth of a minor groove is defined as $d^* = d/D$, where d and D are defined in Fig. 1. The number of the minor grooves per major groove is denoted by n

d^*	D (Å)	d (Å)	n
0.80	9.0	7.2	0, 5, 9
0.83	10.7	8.9	0, 5, 9
0.88	14.3	12.5	0, 5, 9

The widths of the major and minor grooves were fixed to 23.2 and 5.4 Å, respectively.

grooves (n = 9) have low activation free energies <2.4k_BT. In particular, the activation free energy vanishes in the case with the deepest minor grooves (d^* = 0.88). This substantial decrease in the activation free energy of dewetting presumably explains the lotus effect. The water density profiles of the stable CB states corresponding to a, b, and c in the top panel are drawn in the bottom of Fig. 4. These hierarchical grooves are in the CB–CB states, which are necessary to impart the lotus effect.[43,44] For the surface with d^* = 0.88 (c), water molecules are not layered but dried on the top of the minor grooves.

The hierarchical grooves engraved with the minor grooves, which are relatively shallow, wide, and sparse, were explored (Fig. 5). Here, the minor groove depths, d^*, are 0.0, 0.2, 0.4, and 0.8. Depending on d^*, the stable state is either the WZ–WZ or WZ–CB state (Fig. 5, inset). The activation free energies of the wetting transitions are larger (by 3.9k_BT at least) than those of the dewetting transitions (<1.9k_BT). Note that the acti-

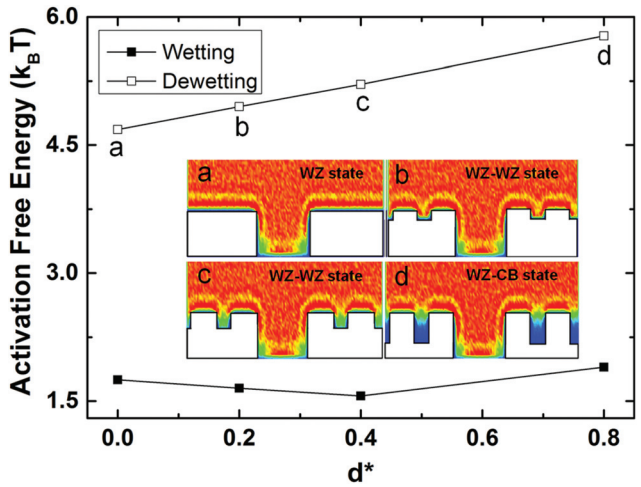

Fig. 5 Activation free energies of the dewetting (open squares) and wetting (filled squares) transitions for the hierarchical grooves with wide and sparse minor grooves. By fixing n to three, the activation free energies of the dewetting and wetting transitions are plotted *vs.* the minor groove depth (d^*). The minor groove depth d^* was varied as 0.0, 0.2, 0.4, and 0.8, by fixing the minor groove width (w^*) to 0.384. The water density profiles of the stable states corresponding to (a), (b), (c), and (d) are shown in the inset. The lines are drawn as a visual guide.

vation free energy for the dewetting transition increases monotonically from 4.7 to $5.8k_BT$ with increasing d^* from 0 to 0.8. This substantial enhancement ($1.1k_BT$) in the activation free energy of dewetting with the minor grooves presumably gives rise to the rose petal effect. The density profile in the inset shows that in this case the WZ–CB composite state is the stable state, which was previously found to exhibit the rose petal effect.[9,15,45] The density profiles illustrate the layering of water molecules near the groove surfaces, even inside the minor grooves for the WZ–WZ states. Note that the liquid water also penetrates slightly down into the minor grooves for the WZ–CB state.

Admittedly, the present simulation, owing to the size limit of an atomistic MD simulation, considered grooves smaller than those in real experiments. We think however that the sizes of the grooves are still big enough to exhibit the essential features of the phase transitions of confined fluids, as the numerous MD simulation studies have previously proved.[24,46–48] Note that our simulation exactly reproduced the composite wetting states (the CB–CB and WZ–CB states) which were experimentally found to exhibit the lotus leaf and rose petal effects.[9,16,49,50] Besides, we deliberately reported the free energies of the (de)wetting transitions in terms of the size-independent quantities: the filling level Z and the relative depth of minor grooves, d^* (= d/D). The present d^* values can be used to predict the micrometer-scale experimental geometries (d and D values) optimal for the lotus leaf and rose petal effects. In addition, the free energy barrier of the dewetting can estimate the work of adhesion of a water drop on a grooved surface. For example, the dewetting of the hierarchical groove with a rose petal effect (d^* = 0.8 in Fig. 5) has a free energy barrier of 3.432 kcal mol^{-1}. As this transition involves a loss of the liquid–solid contact area of 13.18 nm^2 (note that only the major groove is dewetted in the transition), the free energy barrier per unit area is given by 0.0018 J m^{-2}. This value is about 5 times smaller than the work of adhesion measured for a water droplet on a graphene sheet, 0.0096 J m^{-2}.[51] The free energy barrier per unit area refers to dewetting of the major grooves, not to the complete detachment of a water drop from the surface. Therefore, the present free energy barrier per unit area provides a lower bound to the actual work of adhesion. These insights on the optimal geometries and adhesion free energies of the grooved surfaces have potential applications as theoretical principles for designing superhydrophobic grooved surfaces.

The present wetting transition can be viewed as a heterogeneous nucleation of a liquid inside a groove. It will be certainly interesting to check the critical size of such a nucleation of the wetting state. To do so, the dynamics of the wetting transition needs to be closely followed. The present simulation however controls the degree of wetting by restraining the filling level Z and focuses on sampling the configurational space for the free energy calculation. Therefore, the present simulation cannot be used to estimate the critical nucleus needed for the wetting transition. We note however that the previous MD simulation[24] reported that the wetting of a groove proceeds rapidly once the groove is half-filled with a liquid. We therefore estimate that the half volume of a groove is the critical size of the nucleation needed for the wetting of the groove.

Conclusions

The fundamental understanding of the (de)wetting transition of a hierarchical groove has important implications for the design of superhydrophobic surfaces. Currently, the metastable, transition, and intermediate states involved in the (de)wetting transition are largely unknown. In particular, although hierarchical grooves can provide both a low and a high water adhesion strength, which manifests in a lotus leaf and rose petal, respectively, the underlying reasons for these contrasting water adhesion properties are unknown. In this viewpoint, the present all-atom MD simulation study uncovered the free energy profiles for the (de)wetting transitions of single- or dual-scale grooves. A sagging or depinning surface of the liquid penetrating into the grooves was found. With the minor grooves, which are narrow, deep, and densely populated, the dewetting (WZ-to-CB) transition showed a vanishing activation free energy. On the other hand, with minor grooves sparse and wide, the activation free energy of the dewetting transition increased significantly. The increased and decreased activation free energies of dewetting with the minor grooves are related to the contrasting water adhesion properties observed for lotus leaves and rose petals.

Conflicts of interest

There are no conflicts to declare.

Acknowledgements

This study was supported by the National Research Foundation of Korea Grant funded by the Korean Government (no. NRF-2015R1A2A2A01004208 and NRF-2014R1A4A1001690).

Notes and references

1 J. Chapman and F. Regan, *Adv. Eng. Mater.*, 2012, **14**, B175–B184.
2 Y. H. Ghymn, K. Jung, M. Shin and H. Ko, *Nanoscale*, 2015, **7**, 18642–18650.
3 H. Lee, M. L. Alcaraz, M. F. Rubner and R. E. Cohen, *ACS Nano*, 2013, **7**, 2172–2185.
4 A. K. Sasmal, C. Mondal, A. K. Sinha, S. S. Gauri, J. Pal, T. Aditya, M. Ganguly, S. Dey and T. Pal, *ACS Appl. Mater. Interfaces*, 2014, **6**, 22034–22043.
5 N. Liu, Y. Cao, X. Lin, Y. Chen, L. Feng and Y. Wei, *ACS Appl. Mater. Interfaces*, 2014, **6**, 12821–12826.
6 L. Wu, L. Li, B. Li, J. Zhang and A. Wang, *ACS Appl. Mater. Interfaces*, 2015, **7**, 4936–4946.
7 X. Su, H. Li, X. Lai, L. Zhang, T. Liang, Y. Feng and X. Zeng, *ACS Appl. Mater. Interfaces*, 2016, **9**, 3131–3141.
8 H. Zhu, Z. Guo and W. Liu, *Chem. Commun.*, 2014, **50**, 3900–3913.
9 Z.-H. Yang, F.-C. Chien, C.-W. Kuo, D.-Y. Chueh and P. Chen, *Nanoscale*, 2013, **5**, 1018–1025.
10 S. Hoshian, V. Jokinen, V. Somerkivi, A. R. Lokanathan and S. Franssila, *ACS Appl. Mater. Interfaces*, 2014, **7**, 941–949.
11 X. Yu, Q.-Z. Zhong, H.-C. Yang, L.-S. Wan and Z.-K. Xu, *J. Phys. Chem. C*, 2015, **119**, 3667–3673.
12 T. Lv, Z. Cheng, D. Zhang, E. Zhang, Q. Zhao, Y. Liu and L. Jiang, *ACS Nano*, 2016, **10**, 9379–9386.
13 J. T. Han, B. K. Kim, J. S. Woo, J. I. Jang, J. Y. Cho, H. J. Jeong, S. Y. Jeong, S. H. Seo and G.-W. Lee, *ACS Appl. Mater. Interfaces*, 2017, **9**, 7780–7786.
14 L. Jiang, Y. Zhao and J. Zhai, *Angew. Chem., Int. Ed.*, 2004, **116**, 4438–4441.
15 L. Feng, Y. Zhang, J. Xi, Y. Zhu, N. Wang, F. Xia and L. Jiang, *Langmuir*, 2008, **24**, 4114–4119.
16 C. Yuan, M. Huang, X. Yu, Y. Ma and X. Luo, *Appl. Surf. Sci.*, 2016, **385**, 562–568.
17 Z. Cheng, M. Du, H. Lai, N. Zhang and K. Sun, *Nanoscale*, 2013, **5**, 2776–2783.
18 A. U. Zillohu, R. Abdelaziz, S. Homaeigohar, I. Krasnov, M. Müller, T. Strunskus and M. Elbahri, *Sci. Rep.*, 2014, **4**, 7407.
19 T. Sun and G. Qing, *Adv. Mater.*, 2011, **23**, H57–H77.
20 R. N. Wenzel, *Ind. Eng. Chem.*, 1936, **28**, 988–994.
21 A. Cassie and S. Baxter, *Trans. Faraday Soc.*, 1944, **40**, 546–551.
22 A. Giacomello, M. Chinappi, S. Meloni and C. M. Casciola, *Phys. Rev. Lett.*, 2012, **109**, 226102.
23 P. R. Jones, A. T. Kirn, Y. D. Ma, D. T. Rich and N. A. Patankar, *Langmuir*, 2017, **33**, 2911–2919.
24 Z. Zhang, H. Kim, M. Y. Ha and J. Jang, *Phys. Chem. Chem. Phys.*, 2014, **16**, 5613–5621.
25 H. Berendsen, J. Grigera and T. Straatsma, *J. Phys. Chem.*, 1987, **91**, 6269–6271.
26 P. S. Crozier, R. L. Rowley and D. Henderson, *J. Chem. Phys.*, 2001, **114**, 7513–7517.
27 P. R. Pandey and S. Roy, *J. Phys. Chem. Lett.*, 2013, **4**, 3692–3697.
28 M. P. Allen and D. J. Tildesley, *Computer Simulation of Liquids*, Clarendon Press, Oxford, 1987.
29 J.-P. Ryckaert, G. Ciccotti and H. J. Berendsen, *J. Comput. Phys.*, 1977, **23**, 327–341.
30 W. G. Hoover, *Phys. Rev. A*, 1985, **31**, 1695.
31 S. Nosé, *J. Chem. Phys.*, 1984, **81**, 511–519.
32 G. M. Torrie and J. P. Valleau, *J. Comput. Phys.*, 1977, **23**, 187–199.
33 S. Kumar, J. M. Rosenberg, D. Bouzida, R. H. Swendsen and P. A. Kollman, *J. Comput. Chem.*, 1992, **13**, 1011–1021.
34 B. Roux, *Comput. Phys. Commun.*, 1995, **91**, 275–282.
35 A. Grossfield, *WHAM: The Weighted Histogram Analysis Method, 2.0.8*, Grossfield Lab, Rochester, NY, 2013.
36 S. Plimpton, *J. Comput. Phys.*, 1995, **117**, 1–19.
37 G. A. Tribello, M. Bonomi, D. Branduardi, C. Camilloni and G. Bussi, *Comput. Phys. Commun.*, 2014, **185**, 604–613.
38 H. Kusumaatmaja, M. Blow, A. Dupuis and J. Yeomans, *EPL*, 2008, **81**, 36003.
39 Y. C. Jung and B. Bhushan, *Langmuir*, 2008, **24**, 6262–6269.
40 H.-M. Kwon, A. T. Paxson, K. K. Varanasi and N. A. Patankar, *Phys. Rev. Lett.*, 2011, **106**, 036102.
41 N. A. Patankar, *Langmuir*, 2010, **26**, 8941–8945.
42 D. H. Kwon and S. J. Lee, *Appl. Phys. Lett.*, 2012, **100**, 171601.
43 Y. C. Jung and B. Bhushan, *ACS Nano*, 2009, **3**, 4155–4163.
44 B. Bhushan and E. K. Her, *Langmuir*, 2010, **26**, 8207–8217.
45 A. Fernández, A. Francone, L. H. Thamdrup, A. Johansson, B. Bilenberg, T. Nielsen, M. Guttmann, C. M. Sotomayor Torres and N. Kehagias, *ACS Appl. Mater. Interfaces*, 2017, **9**, 7701–7709.
46 T. Koishi, K. Yasuoka, S. Fujikawa, T. Ebisuzaki and X. C. Zeng, *Proc. Natl. Acad. Sci. U. S. A.*, 2009, **106**, 8435–8440.
47 H. Kim, S. I. Lee, M. A. Matin, Z. Zhang, J. Jang, M. Y. Ha and J. Jang, *J. Phys. Chem. C*, 2014, **118**, 26070–26079.
48 Z. Zhang, M. A. Matin, M. Y. Ha and J. Jang, *Langmuir*, 2016, **32**, 9658–9663.
49 B. Bhushan and M. Nosonovsky, *Philos. Trans. R. Soc. London, Ser. A*, 2010, **368**, 4713–4728.
50 M. Afsal and L.-J. Chen, *J. Mater. Chem.*, 2011, **21**, 18061–18066.
51 C.-T. Hsieh and W.-Y. Chen, *Surf. Coat. Technol.*, 2011, **205**, 4554–4561.

